Natural vs engineering CO_2 capture and utilization

Guillermo Galán[a], Mariano Martín[a1], and Ignacio E. Grossmann[b]

[a] Department of Chemical Engineering, University of Salamanca, Plz Caídos 1-5, 37008, Salamanca, SPAIN
[b] Department of Chemical Engineering, Carnegie Mellon University, 5000 Forbes Ave, Pittsburgh PA, U.S.A.

Abstract

In this work, a mathematical optimization approach is used to analyze facilities that capture CO_2 artificially or use the naturally captured CO_2 in the form of lignocellulosic biomass. They are later compared towards the production of methanol evaluating different biomasses including energy crops, forest and agricultural residues, and two direct air capture technologies (DAC). Hydrogen is produced by splitting water using solar and/or wind energy. Facilities based on PV solar and wind turbines have been designed, considering their monthly operation due to the solar and wind availability using a multiperiod approach to provide for the energy to power the DAC's and the production of hydrogen. The current development of technologies gives biomass an advantage as carbon capture technology with production and investment costs 10 times lower due to the large cost of the renewable energy collection for the operation of the fans. However, the area required for growing biomass, but the case of residues, and the total amount of water consumed, 2 orders of magnitude above, are in favor of the engineered alternative.

Keywords: CO_2 capture, solar energy, wind energy, PV, aerogenerator, biomass, water electrolysis

1.-Introduction

[1] Corresponding author: mariano.m3@usal.es

The rapid increase in CO_2 emissions derived from the development of industry, transportation, and other activities, such as agriculture and livestock, as well as their accumulation in the atmosphere, have resulted in the increase of its concentration up to 400 ppm, with a rate of about 1.9 ppm per year since 2009 (Tans, 2009). A local and global increase in temperatures due to the greenhouse effect has been measured. Generally, the temperature has increased 1ºC above pre-industrial levels with consequences, such as sea-level rise, melting of the arctic ice and glaciers, and higher frequency of extreme meteorological phenomena such as torrential rains and hurricanes, prolonged droughts, and heavy snowfalls, among others (Seneviratne, 2012). To reduce and minimize the effects of greenhouse gas emissions and the impact of climate change, the governments of 195 countries committed to adopting 2015 the Paris Climate Agreement, where there is an agreement to limit the increase in temperature to 1.5 °C (Allen et al., 2020) (UN, 2015). Achieving this goal implies drastically reducing CO_2 emissions by 2030 and net zero emissions by 2050. A large amount of CO_2 is produced annually, more than 32 $GtCO_2$ are emitted (EPA Gov, 2019), which makes the development of technology necessary to capture it directly from the atmosphere. Over the last years, there has been a technological effort towards CO_2 capture to reduce the levels in the atmosphere. Currently, there are 65 commercial carbon capture and storage (CCS) facilities globally (Global CCS Institute, 2020). These facilities capture the CO_2 from the concentrated sources and store it in geological deposits, with the risk of leaks over time. As an alternative, the Carbon Engineering (CE) technology (Lackner et al., 1999; Lackner, 2009) employs a process very similar to the used in the 1950s in submarines and spaceships in their closed-circuit breathing systems (Carey et al., 1983). It allows capturing the CO_2 from the atmosphere employing a large number of fans to move the air through alkaline solutions (Lackner, 2009; Keith et al., 2018) capturing the CO_2 using a cycle of reactions of CaO and $Ca(OH)_2$ (Lackner et al., 1999). This CO_2 capture technology is feasible from a thermodynamic and energetic point of view; however, recovering CO_2 from a source as dilute as atmospheric air has the disadvantage of using large volumes of air to extract a significant amount of CO_2. This entails the need to use a large number of fans, with the corresponding energy consumption, and readjust the pH of the capture solutions. To overcome this issue, during the last years of the 2010s, the Bipolar Membrane Electrodialysis **(**BPMED) technology was being studied to recover the dissolved CO_2 without the need for any

cycle of reactions. It is based on the use of cells provided with a bipolar membrane (BPM) and an anion exchange membrane (AEM) that separates the different ions from the stream water fed and the solution (Sabatino et al., 2020).

However, although there are alternatives to capture the CO_2 emitted, it is necessary to sequester it and put it to use. Lately, CO_2 has also been reused as a carbon source. The department of energy in the US presented a diagram of possible services for the captured CO_2 (NETL, 2014) from direct use in the food industry, i.e., carbonated beverages, to its use as extractant, refrigerant, fire suppression or inerting agent, enhanced fuel recovery, and for chemicals, polymers and fuels production. CO_2 can be a raw material for producing urea, polycarbonates, and bulk chemicals such as methanol or methane. Several papers have shown various processes for the transformation of CO_2 into different chemicals via hydrogenation (Kondratenko et al., 2013), including methane (Davis and Martin, 2014 a,b), methanol (Martin & Grossmann, 2016 a,b; Mbatha, 2021), or DME (Martin, 2016 a). To do so, a reduction of CO_2 is required. However, that process is what plants have been doing for ages. Nowadays, biomass-based fuels use the CO_2 fixed by the plants in hydrocarbons to produce bioethanol, biodiesel, etc. (Martin & Grossmann, 2013). If we focus on non-food-linked raw materials, we can talk about algae and lignocellulosic raw materials like switchgrass or residues, for instance. One of the examples that can be produced from both, CO_2 or biomass, is dimethyl ether (DME), a substitute for diesel. It is possible to produce it from biomass-based syngas (Peral et al., 2015) or to obtain it from CO_2 and renewable hydrogen (Martin, 2016 a). It is paramount for the comparison that the energy source is renewable. In this perspective work, we compare both processes to see the performance of the technologies to reuse the CO_2, the one Nature uses and the engineered one to transform solar or wind energy into power using PV panels or wind turbines facilities (Martin, 2017).

This work deals with the mathematical optimization of different methods of capturing CO_2 from atmospheric air, the subsequent synthesis of methanol as the chemical compound of interest, and their comparison with the methanol produced from the gasification of different biomasses. The processes are modelled unit by unit using first principles and experimental data to provide the capability of optimizing the

operating conditions. The rest of the work follows the following structure: Section 2 presents the overall description of the superstructure of the different alternatives to CO_2 capture. Section 3 shows the description for each of the technologies and steps of the different models. Section 4 describes the procedure followed to find the solution. Section 5 summarizes the main results of the study, including the process design and the economic evaluation for all of the CO_2 capture technologies and the source of energy that feeds them. The study analyses 8 different biomasses such as switchgrass, corn stover, miscanthus, wheat straw, and biomass of forestry origin, like pine and spruce bark. In Section 6 the conclusions of the study are summarized.

2.-Processes description and design approach.

This section describes two types of processes to remove CO_2 from the atmosphere, the growing of biomass and its further gasification to produce methanol and the direct air capture of CO_2 and its hydrogenation towards methanol. Due to the low concentration of CO_2 in the atmosphere for industrial applications, 400ppm, it is necessary to move large volumes of air into the installation. The air is introduced through a counterflow air-contactor fitted with a set of fans integrated into a Brentwood-packed tower XF12560 (Holmes & Keith, 2012, Keith et al., 2018). On the one hand, the capture methods are generally based on the conventional process designed by Lackner in 1999 (Lackner et al., 1999), which captures the CO_2 through a cycle of reactions based on alkaline solutions of NaOH (Lackner, 2009). Subsequent modifications carried out by David Keith (Keith et al., 2018) use KOH. The yield of the capture process varies with the system, the contact between the gas and liquid phases, and the solubility of CO_2, but typically takes a value of around 74.5% (Keith et al., 2018). Then, the regeneration of the solution is carried out employing several reactions based on CaO and $Ca(OH)_2$ (Lackner et al., 1999). The CO_2 reacts with a solution of $Ca(OH)_2$ in a pellet reactor forming $CaCO_3$, and KOH, which is recycled to the air contactor. The $CaCO_3$ follows a drying step in a slaker unit where the hydration of CaO to $Ca(OH)_2$ is carried out simultaneously with a conversion of around 85%, being the rest of CaO converted in a later mixing stage with water (Keith et al., 2018). The significant amount of heat produced in this unit is employed to obtain steam, which generates energy in a high-medium pressure turbine (Keith et al., 2018).

On the other hand, in the 2010s, the capture of CO_2 using bipolar electrolysis membranes was developed. Utilizing ion exchange membranes (Sabatino et al., 2020), it is possible to regenerate the alkaline solution without complex chemical cycles of reactions. An anionic exchange membrane (AEM) divides the cell into basic and acid compartments. The basic compartment contains a solution of CO_2 in the form of HCO_3^- and CO_3^{2-} ions. Across the membrane, the acid compartment has a solution of H_3PO_4 at pH between 2.5-2.8 (Eisaman et al., 2011). Thus, when the HCO_3^- and CO_3^{2-} ions move through the AEM, the low pH in acid solution converts them in CO_2, being released as bubbles. A bipolar membrane (BPM) splits the water into H^+ and OH^- ions employing electrical energy to maintain the pH. The H^+ ions go to the acid compartment while the OH^- ions go to the basic compartment, which reacts with K^+ ions forming KOH (Sabatino et al., 2020). However, it is necessary to use a large amount of electrical energy due to the low efficiency of the membrane and the lack of proper control of the CO_2 bubbles formed. Improvements in membrane separation efficiency will lead to reducing energy use and costs. The purification of CO_2 is carried out by removing the water in a condenser and molecular sieves units. The purified CO_2 is mixed with renewable electrolytic H_2, produced through PV panels and/or wind turbines (Martin & Grossmann, 2016 a,b). Finally, the mix is fed to a reactor where methanol production is carried out and its subsequent purification in a distillation column stage.

Alternatively, biomass gasification can also be used. Different biomasses, energy crops as well as waste streams from farms and forestry operations are gasified. Direct or indirect gasification can be used followed by reforming, either steam reforming or partial oxidation. The syngas is to be adjusted in its H_2 to CO ratio for the synthesis of methanol. Next, a fraction of the CO_2 is removed by allowing a 2-8% CO_2 concentration in the syngas that is fed to the synthesis reactor. Methanol is purified before storage. The superstructure that includes all the alternatives presented for the different processes is shown in Figure 1.

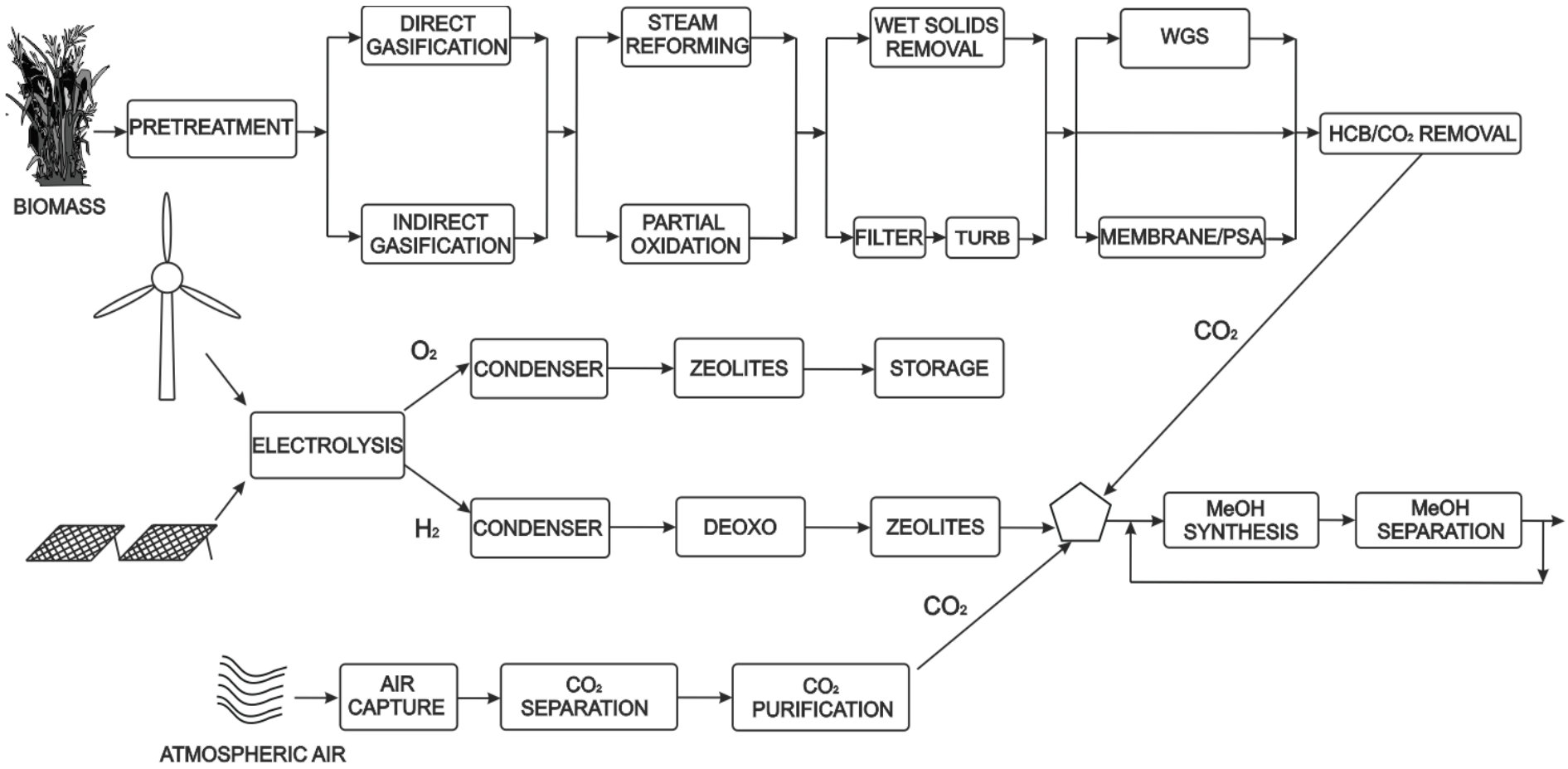

Fig 1. Superstructure for the CO_2 capture from atmosphere.

3.- Modelling

All the operations required for the capture of CO_2 and its transformation into methanol are modelled with mass and energy balances, experimental yields, thermodynamic and chemical equilibrium, and rules of thumb (Martín, 2016a). Surrogate models are developed to model complex units such as biomass gasification and direct air capture, taking data from experiments or simulations of the units. The superstructure is mathematically formulated using temperatures, total and component mass flows, and component mass fractions as variables. The components in the system are included in two different sets, one used in the direct air capture process and the other for the use of biomass, respectively. In the following stages, the main assumptions used to model the major units are presented.

$J_{Direct\ air\ capture}$ = {Water, CO_2, CO, O_2, H_2, CH_4, Ash, MetOH, Air, H_2CO_3, $(HCO_3)^-$, $(CO3)^{2-}$, OH^-, CaO, $Ca(OH)_2$, $CaCO_3$, KOH}.

$J_{Biomass}$ = {Water, C_6H_6, Tars, CO_2, CO, O_2, N_2, H_2, H_2S, NH_3, CH_4, C_2H_2, C_2H_4, C_2H_6, SO_2, C, H, O, S, N, Olivine, Char, Ash, MetOH}.

3.1. Direct CO_2 capture from air

The capture of CO_2 from the air is carried out employing an air-water contactor, which consists of a fan set that moves air through the bed of an absorption tower. It comes into contact with an alkaline solution to retain as much CO_2 as possible. The power of fans is given by eq (1) (Holmes & Keith, 2012).

$$W_{fans} = \frac{Q_{Air} \cdot \Delta P}{\varepsilon} \tag{1}$$

The total power consumed by the fan set is highly dependent on the electrical efficiency and air velocity, v. The electrical efficiency of the fans, ε, is fixed at a constant value of 68.5% (Keith et al., 2018) for this type of operation. The air velocity varies depending on the chosen area, altitude, pressure, etc. A value of 1.4 m/s is set for this analysis based on literature (Holmes & Keith, 2012; Keith et al., 2018). A cross-flow configuration with

an air horizontal flow and the solution downward flow through the packing is chosen. In general, the efficiency in CO_2 capture reaches 74.5% (Keith et al., 2018).

The pressure drop across the packed tower can be calculated from the following correlation, given by eq (2). This correlation is developed for the specific case of PVC packaging material, Brentwood XF12560 (Holmes & Keith, 2012; Keith et al., 2018).

$$\Delta P = 7.4 \cdot D \cdot v^{2.14} \tag{2}$$

For this model of packed towers, a diameter of 7 m is considered the most suitable.

The air introduced into the packed tower has a CO_2 concentration between 300-600 ppm. In general, the mean value of 400 ppm is taken. Henry's Law, eq (3), determines the amount of CO_2 absorbed in the alkaline solution (Seinfeld and Pandis, 1997).

$$[CO_2] = K_H \cdot P_{CO_2} \tag{3}$$

The concentration of CO_2 in the solution depends on its partial pressure and its Henry's constant. When taking CO_2 from atmospheric air, the partial pressure of CO_2 is fixed, making this a value of $3.95 \cdot 10^{-4}$ bar. However, the value of Henry's constant in water depends on the pH of the medium. To determine the value of that constant, experimental results from Seinfeld and Pandis (1997) have been used. The experimental data follows an exponential trend. However, to improve the fitting, a linearization similar to the Eadie-Hofstee linearization (Lehninger, 2000) was chosen to provide the best fit above pH 4, eq (4).

$$K_H = 8.0868 \cdot \frac{K_H}{pH} - 0.3480 \tag{4}$$

From a pH value above 6, there is an exponential increase in said Henry's constant, so it is recommended to work above this value to maximize CO_2 absorption.

The CO_2 absorbed in the solution is subjected to a set of equilibrium reactions in which the formation of H_2CO_3 occurs, which rapidly decomposes towards HCO_3^- and CO_3^{2-} ions, Eqs (5-11) (Lide, 2005). The value of the equilibrium constants for eq (8-11) is summarized in Table 1.

$$CO_2(aq) + H_2O \overset{K1}{\rightleftharpoons} H_2CO_3(aq) \quad (5)$$

$$H_2CO_3(aq) \overset{K2}{\rightleftharpoons} H^+(aq) + HCO_3^-(aq) \quad (6)$$

$$HCO_3^-(aq) \overset{K3}{\rightleftharpoons} H^+(aq) + CO_3^{2-}(aq) \quad (7)$$

$$H_2O \overset{Kw}{\rightleftharpoons} H^+(aq) + OH^-(aq) \quad (8)$$

$$K_1 = K_H = \frac{[H_2CO_3]}{P_{CO_2}} \quad (9)$$

$$K_2 = \frac{[H^+]\cdot[HCO_3^-]}{[H_2CO_3]} \quad (10)$$

$$K_3 = \frac{[H^+]\cdot[CO_3^{2-}]}{[HCO_3^-]} \quad (11)$$

$$K_w = [H^+]\cdot[OH^-] \quad (12)$$

Table 1.- Equilibrium reaction constants

K_2 (M)	$4.45\cdot10^{-7}$
K_3 (M)	$4.69\cdot10^{-11}$
K_w (M^2)	10^{-14}

From eqs. (5)-(11) for pH values above 8.5, the concentration of H_2CO_3 is minimal, most of the CO_2 is converted to HCO_3^- ion, while at pH values above 11, practically all the H_2CO_3 is in the form of CO_3^{2-} ion. The pH value will be determined based on the amount of CO_2 to be recovered and the reactivity of each species based on the CO_2 capture method used.

3.1.1. Conventional method

This method of CO_2 capture is based on the use of an alkaline solution, which is regenerated through a complex chemical cycle based on CaO and its precipitation as $CaCO_3$ (Lackner et al., 1999). This method was improved lately by David Keith, where NaOH was changed by KOH that facilitates the capture of CO_2 and the subsequent regeneration of the solution. The process was named Carbon Engineering (CE) (Keith et al., 2018), and it is shown in Figure 2.

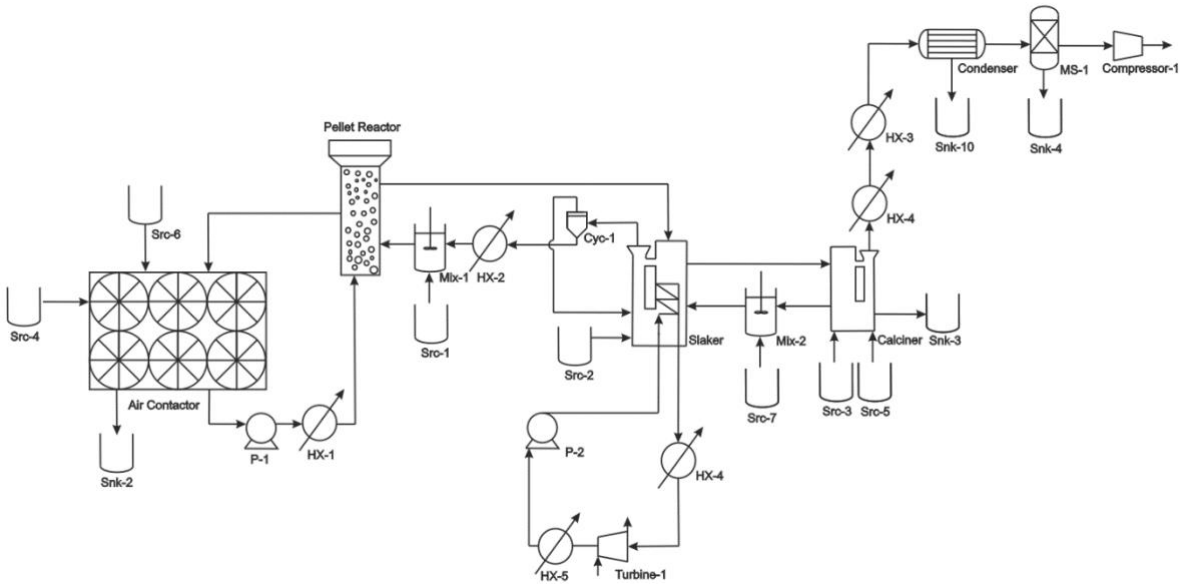

Fig 2. Carbon Engineering process (conventional DAC process)

In this process, the atmospheric air enters the facility through a set of fans that put said the air in contact with an alkaline KOH solution. Due to the addition of KOH, the pH of the solution increases, being able to improve the capture of CO_2 based on what is established in eqs. (5)-(12). The overall reaction can be expressed from eq (13) (Keith et al., 2018).

$$CO_2(\mathrm{g}) + 2KOH(\mathrm{aq}) \rightarrow H_2O(\mathrm{l}) + K_2CO_3(\mathrm{aq}) \qquad \Delta H = -95.8\ \mathrm{kJ \cdot mol^{-1}} \qquad (13)$$

The formation of K_2CO_3 occurs due to the increase in pH, which causes the balance of CO_2 to shift towards the formation of CO_3^{2-}. It reacts with the K^+ ion forming the salt. Subsequently, the regeneration of the alkaline solution takes place in a pellet-type reactor, where the contact of K_2CO_3 with a solution of $Ca(OH)_2$ occurs,

forming $CaCO_3$ and regenerating the KOH, which is recirculated back to the air-water contactor to continue capturing CO_2. The reaction in the pellet reactor can be expressed from eq (14) (Keith et al., 2018).

$$K_2CO_3(\text{aq}) + Ca(OH)_2(\text{aq}) \rightarrow 2KOH(\text{aq}) + CaCO_3(\text{s}) \downarrow \qquad \Delta H = -5.8\ \text{kJ}\cdot\text{mol}^{-1} \tag{14}$$

Once the $CaCO_3$ is formed, it precipitates due to its low solubility in water, which favors its separation from the solution (Sabatino et al., 2020). Once the solution is separated, the $CaCO_3$ that remains with the residual water (12% w/w) and the KOH impurities are sent to the slaker, where it is dried. In this equipment, the drying of $CaCO_3$ has been produced and the production of steam around 300ºC, which will be used to produce energy in a medium pressure turbine, Turbine-1.

The next stage consists of the calcination of the $CaCO_3$ in the calciner to release the CO_2, eq (15). (Sanz-Pérez et al, 2016)

$$CaCO_3(\text{s}) \rightarrow CaO(\text{s}) + CO_2(\text{g}) \qquad \Delta H = 179.2\ \text{kJ}\cdot\text{mol}^{-1} \tag{15}$$

Since this reaction is very endothermic and requires temperatures close to 900ºC, methane is typically used as fuel (Sabatino et al., 2020). However, in an attempt to avoid the use of fossil resources, biogas can be used (Martín-Hernández et al., 2020) (León & Martin, 2016). All the CO_2 it contains, and that is produced in its combustion, can be mixed with the CO_2 captured from the environment, thus avoiding its emission. 98% regeneration can be achieved (Keith et al., 2018), saving the rest for future feeds.

Then the next stage consists of hydrating the CaO produced in the calciner to produce the $Ca(OH)_2$ that allows the KOH to be regenerated from the alkaline solution. (Sanz-Pérez et al., 2016).

$$CaO(\text{s}) + H_2O(\text{l}) \rightarrow Ca(OH)_2(\text{s}) \qquad \Delta H = -64.5\ \text{kJ}\cdot\text{mol}^{-1} \tag{16}$$

The conversion of CaO for this reaction is usually around 85%, a subsequent hydration stage being necessary to make all the CaO react (Keith et al., 2018).

3.1.1.1. Medium-low pressure turbine

The Turbine-1 employs a Rankine cycle to generate electrical energy using steam expansion to reduce the external use and minimize the energy cost. A stream of water is fed through an external circuit in the calciner. The reaction heat released is employed to heat up this water to produce medium pressure steam, between 20 bar and 47 bar (Martin & Martin, 2017). Later, this steam is converted to superheated steam when used to cool the CO_2-rich stream leaving the calciner. The steam is eventually fed into the turbine, where the enthalpy it contains is used to generate electricity. The resulting steam is condensed using cooling water and its pressure is increased by a pump. The modeling of the medium-low pressure steam turbine is based on León & Martin (2016).

3.1.2. Bipolar membrane electrodialysis (BPMED)

This CO_2 capture method bases its operation on bipolar electrodialysis membranes. Unlike the conventional process, the regeneration of the saline solution does not use a chemical cycle of reactions but the use of ion-exchange membranes driven by an electrical potential. Figure 3 shows the scheme of the process.

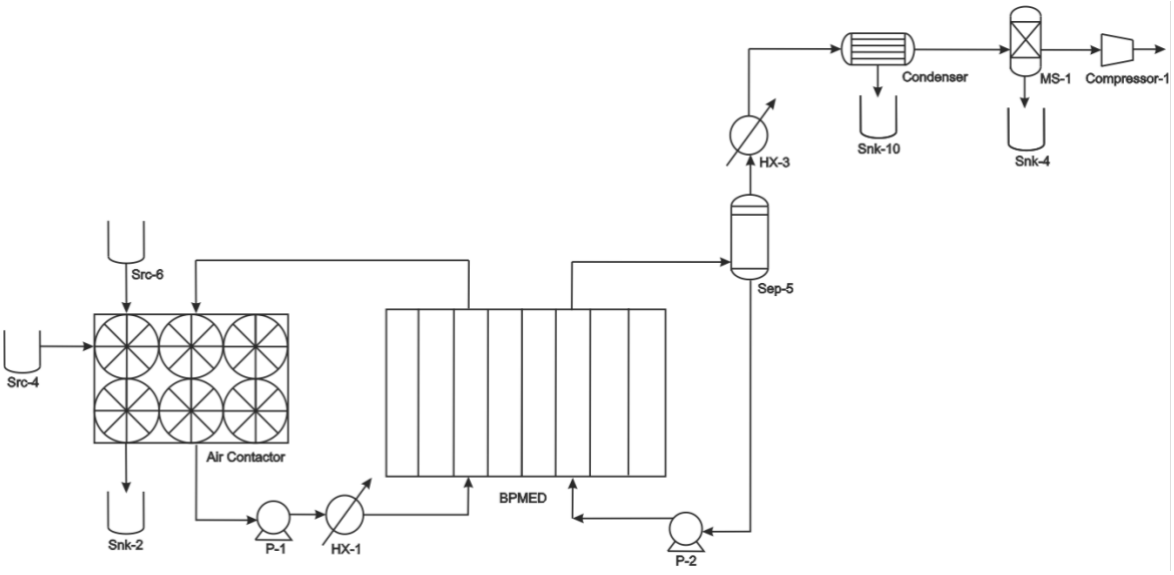

Fig 3. BPMED carbon capture process.

In general, a simple cell structure consisting of a bipolar type membrane (BPM) that allows the separation of H^+ and OH^- ions from water and an anion exchange membrane (AEM) is used. With this division, the cell has acid and basic compartments. Figure 4 shows a scheme of the cell structure (Sabatino et al., 2020).

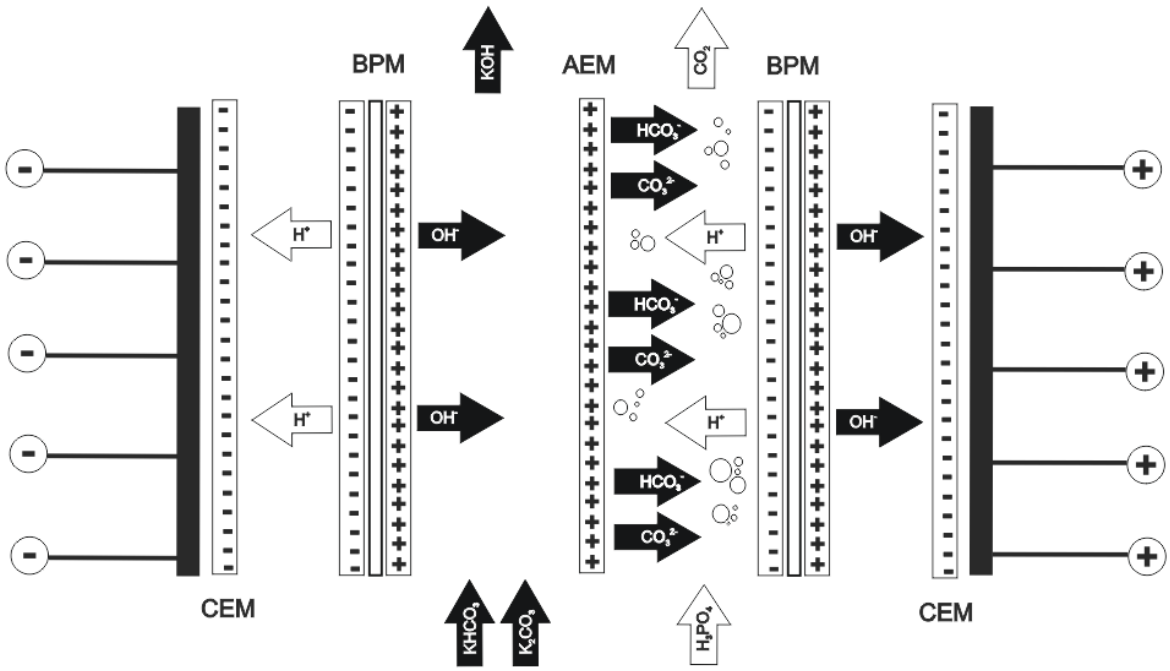

Fig 4. Structure of the BPMED cell

The CO_2 captured from the air is found in solution in the form of HCO_3^- and CO_3^{2-} ions together with K^+. The solution rich in both ions is fed to the basic compartment of the cell, while a buffer solution composed of H_3PO_4 at pH 2.5-2.8 is fed to the acid compartment (Eisaman et al., 2011). On the one hand, the use of an electric current through the BPMs allows to split the water in H^+ and OH^-. In the basic compartment, the K^+ and OH^- react between them, regenerating the KOH in the basic solution, eq (17) (Lide, 2005). The heat generated in the reaction produces a slight increase in the temperature of the solution by 0.08ºC, which is not taken into account because it does not produce significant temperature variations.

$$K^+(\text{aq}) + OH^-(\text{aq}) \rightarrow KOH(\text{aq}) \qquad \Delta H = -412.71\ \text{kJ}\cdot\text{mol}^{-1} \tag{17}$$

On the other hand, the HCO_3^- and CO_3^{-2} ions move to the acid compartment across the AEM. Based on eqs. (10)-(12) at pH values below 4, the distribution of chemical species is mainly in the form of CO_2, which is released

as bubbles (Sabatino et al., 2020). These bubbles can increase the resistance of the cell, thus being necessary to use more significant electrical potential and therefore a greater consumption of electricity.

To calculate the power consumption in the cell, it is necessary first to calculate the molar flow rate of CO_2 through the membrane eq (18) is employed (Sabatino et al., 2020).

$$J_{CO_2} = \frac{i \cdot S}{F} \cdot \eta \tag{18}$$

From the data of Sabatino et al. (2020), the molar flow rates as a function of the current density, i (A/m^2), and concentrations of KOH and HCO_3^- and CO_3^{-2} ions can be expressed as a surface response model, eq (19).

$$\begin{aligned} J_{CO_2} &= 9.8 \cdot 10^{-5} + 10^{-6} \cdot i + 1.94 \cdot 10^{-3} \cdot [HCO_3^-] + 2.66 \cdot 10^{-4} \cdot [CO_3^{2-}] + 3.3 \cdot 10^{-4} \cdot [KOH] \\ &-3.8 \cdot 10^{-3} \cdot [HCO_3^-] \cdot [HCO_3^-] - 1.15 \cdot 10^{-4} \cdot [CO_3^{2-}] \cdot [CO_3^{2-}] + 2 \cdot 10^{-6} \cdot i \cdot [HCO_3^-] - 6 \cdot 10^{-6} \cdot i \cdot [KOH] \\ &- 2.6 \cdot 10^{-3} \cdot [HCO_3^-] \cdot [CO_3^{2-}] \end{aligned} \tag{19}$$

The current efficiency can also be expressed as a surface response model dependent on the last same variables. To build the model showed the data have taken from Sabatino et al. (2020).

$$\begin{aligned} \eta &= 0.2972 + 0.000102 \cdot i + 4.89 \cdot [HCO_3^-] + 0.4377 \cdot [CO_3^{2-}] - 4.8336 \cdot [KOH] \\ &-7.40 \cdot [HCO_3^-] \cdot [HCO_3^-] - 0.1936 \cdot [CO_3^{2-}] \cdot [CO_3^{2-}] + 8.049 \cdot [KOH] \cdot [KOH] \\ &+ 1.89 \cdot 10^{-4} \cdot i \cdot [HCO_3^-] + 6 \cdot 10^{-6} \cdot i \cdot [CO_3^{2-}] - 9.2 \cdot 10^{-5} \cdot i \cdot [KOH] - 5.35 \cdot [HCO_3^-] \cdot [CO_3^{2-}] \end{aligned} \tag{20}$$

To improve the data fit, the current density has been limited to between 200-1000 A/m^2 due to the maintenance of the data trend.

However, the voltage losses have a significant influence on the power consumption in the cell. This is given by eq. (21)

$$E_{Cell} = i \cdot R_{Cell} + E_{BP} \tag{21}$$

To reduce the voltage drops in the cell is necessary to reduce the cell resistance for a given value of current efficiency because the water-splitting potential of the BPM, E_{BP}, has a constant value for the cell. The cell resistance is provided by eq (22).

$$R_{Cell} = R_{Base} + R_{AEM} + R_{Acid} \tag{22}$$

The cell resistance can be computed as the contribution of the resistance in both compartments, basic (R_{Base}), and acid (R_{Acid}), respectively, and the resistance in the AEM (R_{AEM}). The resistance in the AEM has a constant value for a given type of membrane. Still, the resistance in the two compartments of the cell depends on the distance between the BPM and the AEM and the electrical conductivity of the solution. This is expressed with eq. (23).

$$R_{Acid,Base} = \frac{\delta}{k_{Acid,Base}} \tag{23}$$

However, the value of the electrical conductivity of the acid solution can change due to the formation of gas bubbles when the CO_2 is released. An increment in the number of bubbles allows reducing the contact between the solution and the membranes, thus reducing the electrical conductivity. This effect is captured with eqs. (24)-(25).

$$\frac{k^*_{Acid}}{k_{Acid}} = \frac{1 + A \cdot B \cdot \varphi_{co_2}}{1 - B \cdot \gamma \cdot \varphi_{co_2}} \tag{24}$$

$$\gamma = 1 + \frac{1 - \varphi_m}{\varphi_m^{\,2}} \cdot \varphi_{co_2} \tag{25}$$

If the CO_2 produced increases, the bubbles will take all the space between the membranes. For this reason, the volumetric fraction of bubbles is limited, achieving a maximum value of 0.637 (Sabatino et al., 2020). Therefore, only the variation in the electrical conductivity of the acid solution can be determined. However, the basic solution also varies. This effect can be captured with the Kolhrausch law (Sivasankar, 2008) to calculate the molar conductivity of the electrolytes, eqs. (26)-(28).

$$\Lambda_m = \Lambda_m^o - E\sqrt{c} \tag{26}$$

$$\Lambda_m = \frac{k_{Base}}{c} \tag{27}$$

$$\Lambda_m^o = \sum_{i=1}^{n} \nu_i \cdot \lambda_i^o \tag{28}$$

If the value of the concentration of the electrolytes is very slow, then it can be assumed $\Lambda_m = \Lambda_m^o$. The values of the molar conductivities at infinity dilution are summarised in Table 2 (Sivasankar, 2008) (Lide, 2005).

Table 2.- Molar conductivities at infinity dilution for the ions at 25ºC

Ion	λ^o ($S \cdot m^2 \cdot mol^{-1}$)
H^+	$3.50 \cdot 10^{-2}$
OH^-	$1.98 \cdot 10^{-2}$
K^+	$7.35 \cdot 10^{-3}$
HCO_3^-	$4.45 \cdot 10^{-3}$
CO_3^{2-}	$1.39 \cdot 10^{-2}$

Finally, the power consumption in a single cell is given by eq. (29).

$$P_{Cell} = i \cdot S \cdot E_{Cell} \tag{29}$$

The power consumption would decrease with the reduction of the resistance in the base compartment caused by low concentrations of the ions HCO_3^- and CO_3^{2-}, since the acid compartment has a fixed resistance value when the pH is set. Moreover, the current efficiency depends on the concentrations of the ions, affecting the current density and the single membrane area. The specific energy demand can be determined with the number of membranes and the total power consumption as given by eq. (30).

$$SPEND = \frac{N_{stack} \cdot N_{Cell} \cdot P_{Cell}}{J_{CO_2}} \tag{30}$$

3.2. Water electrolysis

The electrolysis of water is carried out mainly to obtain hydrogen to mix it with the captured CO_2. The reaction that occurs is given by eq (31).

$$H_2O(\mathrm{l}) \rightarrow H_2(\mathrm{g}) + \frac{1}{2}O_2(\mathrm{g}) \qquad \Delta\mathrm{H}= 285.83\ \mathrm{kJ\cdot mol^{-1}} \tag{31}$$

The energy required to carry out the process can come from wind turbines or PV panels. The oxygen-containing stream is saturated with water vapor, as well as having traces of hydrogen. The water is removed by condensation and using an adsorbent zeolite bed. Once the oxygen is dehydrated, it is compressed and stored for use in the plant or sale. The stream that contains most of the hydrogen is also saturated with water along with small traces of oxygen. Most of the water, like the previous oxygen stream, is removed by condensation but then passes through a deoxygenation reactor, in which the traces of oxygen that can damage subsequent synthetic stages are removed. Deoxygenation produces water, which together with the water that could not be removed by condensation is removed with a bed of zeolites. For more details on the modeling of the water electrolysis process, consult Davis and Martin (2014) (Davis & Martín, 2014 a,b).

3.2.1. Wind energy

A commercial wind turbine, the GE 1.5sle turbine model (SAM, 2013), is considered for the analysis. To calculate the power generated by the turbine, eq (32) is used (Davis and Martín, 2014b). The value of $P_{nominal}$ is 1500 kW. The value of v is the mean value of the wind speed in the location of the wind farm, a and m are adjustment parameters that take the values of acquires the value of 8.322 m/s and 0.806 s/m respectively. (de la Cruz and Martín, 2016).

$$P = \frac{P_{No\min al}}{1 + e^{\left(\frac{-(v-a)}{m}\right)}} \tag{32}$$

3.2.2. Solar energy

For this renewable energy source, it is taken as a reference that each photovoltaic panel generates 1 kWp per 8 m^2 (using a 25% efficiency). To calculate eq (33) is used:

$$P = P_{panel} \cdot N_{panel} \cdot \eta_{panel} \quad (33)$$

The costs associated with the installation range from 1,700 $ to 4,000 $/kWp (Goodrich et al., 2012; Maaßen et al., 2011), taking as value for the calculation 2,300 $/kWp (Martin, 2016 b).

3.3. Methanol synthesis

The synthesis of methanol is carried out by mixing the hydrogen of electrolytic origin with the CO_2 obtained from air. The optimal pressure and temperature conditions of the gas mixture are reached utilizing a set of compressors and heat exchangers. The methanol production is regulated by a set of equilibria in the presence of catalysts generally based on $Cu/ZnO/Al_2O_3$. This reaction does not have a complete conversion so the gases that have not reacted are recirculated back to the reaction section while the methanol is purified by distillation and finally stored for sale. For more details on the modeling see (Martin & Grossmann, 2016 a,b).

3.4. Biomass gasification

This alternative is based on biomass gasification (see Figure 1). Firstly, the biomass has to follow a step of washing, removing solids, and milling, reducing the particle size to be appropriate for gasification, increasing contact surface. To gasify the biomass, two technologies can be employed. On the one hand, **The Renugas gasifier (R)** consists of direct gasification of the biomass at medium pressure. The gasifier uses pure oxygen, not air, and steam obtaining raw syngas rich in CO_2 as a result. The correlations from Eggeman (2005) are used to compute the gas composition. This operation allows obtaining a large performance per reactor volume and a significant reduction in the requirements for downstream. Nevertheless, its efficiency is lower (Eggeman, 2005). On the other hand, **Battelle Columbus (Ferco, F)** operates at a lower pressure with indirect heating. The system is composed of two compartments, the gasifier, and the combustor. The energy required for gasification comes

from burning char, which allows the olivine to be heated and sent to the gasifier. The correlations from the literature (Phillips et al 2007) are used to determine the gas composition. The raw syngas obtained contains heavier hydrocarbons and a lower amount of CO_2.

Once the synthesis gas has been produced, the following steps will eliminate the hydrocarbons that may have been generated in the previous gasification stages. A **Steam reforming (S)** is carried out on one side. The operation is endothermic, needing a heating source, but the syngas obtained present a higher hydrogen gas concentration. On the other side, **Partial oxidation (O)** is performed. Unlike the previous one, the operation is exothermic, releasing heat that must be removed to maintain the correct operation of the process. In addition, a synthesis gas with a lower hydrogen concentration is obtained. Literature conversions are used to determine the gas composition (Martín and Grossmann, 2011).

Subsequently, the raw syngas produced must be cleaned. To achieve this objective, two steps can be followed. The first step consists of cold washing using a scrubber system for low-pressure gasification. A ceramic filter with high-temperature capability can also be used for high-pressure gassing operations. The second step consists of an operation with a multilayer PSA system that is used to remove the last traces of hydrocarbons and other compounds and H_2S and CO_2 in that order. The composition of syngas is adjusted for the proper ratio of H_2 to CO, around 2.

Finally, methanol is synthesized. A reaction controlled by the equilibrium, recycling of the unreacted gases is required due to the low conversion per pass. The methanol is purified from the liquid mixture in a distillation column. In this section, the equations corresponding to the modelling of the entire process have been omitted. Further details on the model can be found in Martin and Grossmann (2011, 2018) (see supporting information).

4. Solution procedure

The resolution of the problem was carried out using decomposing the superstructure into nonlinear optimization models (NLP) involving around 2000-2500 equations and 3000 variables each one. A total of 4 processes involving biomass, where the gasifier operating conditions, the temperatures, flows, and pressures

across the flowsheet are the decision variables, and 2 using DAC, where the main decision variables are the membranes' performance, the total flow of CO_2 that passes through them, the intensity of current applied to the CO_2 capture process BPMED, and the concentrations of CO_2, HCO_3^-, CO_3^{2-} and KOH. The models are solved using a multi-start optimization approach in GAMS with CONOPT 3.0 as the preferred solver. The objective function maximizes profits, including the sale of methanol and oxygen produced in the electrolysis of water and the electrical energy and steam consumed at the highest variable cost, eq. (34):

$$Z = P_{MetOH} m_{MetOH} + P_{O_2} m_{O_2} - P_{Electricity} \sum_i W_{consumed} - \sum_i P_{utilities} \cdot m_{utilities} \quad (34)$$

Next, a network of heat exchangers is developed (Yee et al., 1990) and an economic evaluation to determine production and investment costs (Sinnot, 1999). Their production costs involve the annualized cost, utilities, labor needed, raw material used, and the credit obtained from the sale of excess oxygen produced in water electrolysis. The costs related to public services are updated based on what is stipulated in the literature, 19 $\$ \cdot t^{-1}$ steam, 0.057 $\$ \cdot t^{-1}$ cooling water, Electricity: $1.7 \cdot 10^{-8}$ $\$ \cdot J^{-1}$ (Pérez -Uresti et al., 2019). The base price for biomass varies depending on the one chosen for each case; see Table 5.

The investment is calculated by estimation using the factorial method (Sinnot, 1999). First, the cost of the equipment is estimated by sizing the units using the results from the mass and energy balances obtained from the optimization. The cost of equipment such as heat exchangers, separators, tanks, compressors, distillation column, filters, molecular sieves, gasifiers, and mechanical separation is updated using the values calculated through the correlations developed by the authors, see supplementary material by Almena and Martín (2015) and Martín & Grossmann (2011). Then the cost of the equipment is calculated with the cost of the equipment using complementary factors of 3.15 and 1.4, which correspond to the facility that processes fluids and solids for the material and total fixed costs (Sinnot, 1999). The production costs comprise annualized, chemical products used (KOH, CaO, H_3PO_4, and biogas), equipment, utilities, labor, and raw materials.

5.- Results and discussion

The installation is based on a methanol production rate of 13,160 kg/s, a stipulated amount based on the use of a 20 kg/s switchgrass feed as a base case to produce it, which is close to 18 kg/s of biomass used generally in bioethanol production facilities and biomass processing (Martin & Grossman, 2014). For this assessment, the chosen location was the province of Cádiz (Spain) which presents average solar irradiation of 0.6 kW/m^2 and an average air velocity of 7.5 m/s. The monthly values are taken from AEMET (2020). The size of the PV facility and the wind farm is such that allows an average annual production similar to the one obtained with the base case of switchgrass.

5.1.- Facility operation

Tables 3 and 4 summarize the yields within the gasification of biomass and DAC process paths. It is challenging to use these data to directly compare them because the technologies employed are very different. Still, they can be used to compare the yields of different biomasses and the behavior of the two DAC processes. The discussion is first focused on biomass-based processes, Table 3. They have been obtained following indirect gasification linked to steam reforming, the optimal selection of technologies for biomass processing. The H_2 to CO ratio needed for methanol production is high, around 2, which is the main reason for the selection of those technologies. Table 3 shows that the biomasses with a higher ratio $kg_{MetOH}/kg_{biomass}$ are pine and spruce bark. They present a large composition in carbon that also allows using the lowest amount of biomass, reducing the size of the units, the investment, and the production cost (see Table 5). However, the productivity of each biomass presents the opposite behavior. When the carbon composition increases, the requirements in organic material also increase, thus slowing down growth and therefore biomass productivity per unit area if there is no regular access to a carbon source. In addition, productivity is linked to the chosen plant species and the requirements of water to grow. While switchgrass, corn stover, wheat straw, and miscanthus are native herbaceous-type plants or related to a crop with a typical medium average requirement of water in specific periods, pine and spruce bark come from woody-type plants that receive a variable supply of water throughout the year, generally from rainwater. Moreover, with a slower growth rate generally adapted to mountainous environments and with soils with little or no fertilizer. Then, the total

surface required is related to the amount of biomass employed, the productivity of the soil, and the requirements of water, thus having a tradeoff between the cost of the biomass and the land. The requirements of water (Table 3) account for the water that is lost in the streams that leave the process, the water lost by evaporation from the cooling system at the cooling tower, and the water required for the growth of the biomass. The water evaporated is given by eq. (35) (Perry, 1997).

$$m_{EvaporatedWater} = 0.00085 \cdot 1.8 \cdot \Delta T \cdot m_{CoolingNeeds} \quad (35)$$

The difference of temperature between the inlet and outlet water in the refrigeration circuit, ΔT, takes the typical value of 8ºC.

The water requirements of each biomass, $kg_{Required\ water}/kg_{biomass}$ (Table 3) is an influential factor from the point of view of biomass growth but with little importance in terms of costs. This is since all the treated biomass obtains all or a large part of the water necessary for growth through natural irrigation, mostly from rain. Generally, the herbaceous-type biomass presents a large ratio of $kg_{Required\ water}/kg_{biomass}$ and $kg_{Required\ water}/kg_{MetOH}$ because they are plants suitable for food production and crops in generally temperate climates. woody-type plants present variable water requirements depending on the climatic zone and the evaporation rate characteristic of each species. Seeing Table 3 the two biomasses with the larger requirements of water are wheat straw and spruce bark, 1,803.750 $kg_{Required\ water}/kg_{MetOH,}$ and 1,803.713 $kg_{Required\ water}/kg_{MetOH}$ respectively, being a very similar value. If an external contribution of water were necessary due to droughts to increase production, these costs must be considered. Nevertheless, pine and spruce bark need a larger area to be produced, having a tradeoff between the price of the biomass and the amount fed and the surface required to produce the raw material.

Table 3.- Major yields for gasification of different biomasses (A: Yimam et al., 2015; B: García et al., 2017; C: Salim, 2015; D: Dželetović et al., 2013; E: Abad Viñas et al., 2016; F: Bredemeier et al., 2011; G: Alexopoulou et al., 2020; H: Khanna and Paulson, 2016; I: Dai et al., 2016; J: Nolan et al., 2010; K: USDA, 1979; L: Miranda et al., 2017; M: Gryc e al., 2011; N: Brèteau-Amores et al., 2019; O: Liepins and Liepins, 2015).

	Gasification					
	Switchgrass	**Corn Stover**	**Wheat Straw**	**Miscanthus**	**Pine Bark**	**Spruce Bark**
Amount of biomass (kg/s)	20	19.517	21.235	19.146	15.032	16.124
$kg_{MetOH}/kg_{biomass}$	0.658	0.674	0.620	0.687	0.875	0.816

$Kg_{cooling\ needs}/kg_{biomass}$	116.043	120.333	114.561	120.853	131.331	127.156
Growth water (mm)	786[A]	961[B]	815[C]	800[D]	600[E]	600[F]
$kg_{Growth\ water}/kg_{biomass}$	655	880.040	1,116.44	800	864.550	1,470.590
$Kg_{Evaporated\ water}/kg_{biomass}$	1.420	1.473	1.402	1.479	1.607	1.556
$kg_{Required\ water}/kg_{biomass}$	656.420	881.510	1,117.841	801.479	866.161	1,472.145
$kg_{Required\ water}/\ kg_{MetOH}$	997.600	1,307.328	1,803.750	1,166.04	989.372	1803.713
Productivity (t/km^2)	1,200[G]	1,092[H]	730[I]	1,000[J]	694[K,L]	408[M,N,O]
Surface required (km^2)	518.40	559.25	904.79	595.52	673.34	1,229.80

On the other hand, Table 4 shows the major parameters associated with the DAC processes. They both present a similar surface required using PV panels, due to the similar energy consumption. In the case of BPMED 10-15% higher due to the larger consumption of electricity associated with the operation of the membranes and the CO_2 bubbles formed in the acid compartment of the cell. Similar behavior is shown in the case of the use of using wind as a source of energy. The conventional process requires a 15% lower number of turbines and the use of the Turbine-1 reduces the consumption of electricity by 3.76% (Table 4). Focusing only on the capture of CO2, the energy produced by the turbine can provide up to 49% of fans energy consumption. However, the BPMED process presents a higher $kgCO_{2\ air\ captured}/kW$ ratio. This can be explained because BPMED allows modifying the composition and the pH of the solution changing the electrical requirements in the cell. The conventional process is less versatile due to complex cycle reactions, each of which is produced on different equipment. The total CO_2 used in this process comes from the air capture and the combustion of 2.22 kg/s of biogas (0.17 kg_{Biogas}/kg_{MetOH}) in the calciner, obtained generally from manure (León & Martin, 2016; Martín-Hernández et al., 2020). This operation allows increasing the capture by 40.8%. It can be seen that in both cases, the conventional or the BPMED, the $kg_{MetOH}/\ kgCO_{2\ available\ captured}$ is similar, around 1.40. However, the total production of methanol is higher in the conventional, due to the additional source of CO_2, $kg_{MetOH}/CO_{2\ air\ captured}$, being the variation percentage the one described above, 40.8%.

From the point of view associated with water requirements, the conventional process has a lower ratio $kg_{Required\ water}/kg_{MetOH}$ than the BPMED process. This is due to the lower cooling water needs in the process as a consequence of the better energy integration in the heat exchangers and the lower use of water in the air contactor. The BPMED process has better membrane efficiencies in the presence of higher concentrations of

HCO_3^- which forces the pH to be lowered and thereby increases the amount of water used and thus the amounts lost.

Table 4.- Major yields for DAC process paths

		DAC			
		Conventional Process PV panels	**Conventional Process Wind**	**BPMED PV panels**	**BPMED Wind**
Surface required (km^2)	PV panels	2.05	-	2.31	-
Number of units	Wind turbines	-	572	-	643
Power supplied by Turbine-1 (%)		3.76	3.76	-	-
$kgCO_{2\ air\ captured}/kW$		573.60	573.60	867.03	867.03
$kgCO_{2\ available\ captured}/kW$		968.79	968.79	867.03	867.03
$kg_{MetOH}/CO_{2\ air\ captured}$		2.37	2.37	1.39	1.39
$kg_{MetOH}/\ kgCO_{2\ available\ captured}$		1.41	1.41	1.39	1.39
$kg_{Biogas}/\ kg_{MetOH}$		0.17	0.17	-	-
$kg_{Required\ water}/\ kg_{MetOH}$		27.18	27.18	35.44	35.44

5.2.- Economic evaluation

The economic evaluation is carried out for all biomasses and the three technologies, biomass gasification or the two DAC technologies computing the production and investment costs. The discussion comments first the processes based on biomass and moves on to the direct air capture ones. Table 5 summarizes the production and investment costs for the different biomasses. Pine and spruce bark present the lowest investment and production cost among them. This is because they show a higher $kg_{MetOH}/kg_{biomass}$ ratio, resulting in the need for a lower amount of biomass fed to the installation. The lower biomass prices, 75.41 €/$t_{Biomass}$ and 20.35 €/$t_{Biomass}$ respectively, are also in their favor. Wheat straw presents the lowest price within herbaceous-type biomasses, 50 €/$t_{Biomass}$. Generally, the price of the biomass depends on many factors, such as the use of fertilizers, irrigation, costs of collection and transport, quantity produced, losses due to meteorological effects, total surface required to cultivation, etc... However, herbaceous-type biomass can be easily used in the chemical industry due to the ease of operation in pretreatment. Its lignocellulosic structure degrades more quickly than the structure of pine and spruce bark, thus providing less severe conditions in its

pretreatment, explaining why the price of herbaceous biomass is higher. The distribution of production costs is shown in Figure 5 a-d. Herbaceous-type biomass presents almost the exact distribution of the different items: raw materials 50-60%, equipment 15-20%, utilities 15-20%, administration 5-7%, and salaries 6-7%. Wheat straw provides the lowest production and investment cost, 0.170 €/kg_{MetOH} and 157.67 M€, respectively (Table 5). These values are also found for pine bark (Figure 5 e). However, that is not the case for spruce bark (Figure 5 f), which presents a distribution where the raw materials represent the half value respect the rest of biomasses, 23%. Its amount of biomass fed, 16.124 kg/s (Table 3), and its price, 20.35 €/$t_{Biomass}$ (Table 5), allows to reduce the production cost to 0.110 €/kg_{MetOH}, thus being outside the range established in Table 5 for Herbaceous biomasses, 0.170-0.225 €/kg_{MetOH} but in all cases very competitive with current prices, around 0.4 €/t (https://www.methanol.org). Based on the yields (Table 3) and the price, production, and investment cost (Table 5), the best biomasses to use to carry out the gasification process are spruce bark and wheat straw, being able to choose the most suitable biomass depending on the market price or the surface required for its production.

Table 5.- Production costs and investment for gasification of different biomasses (P: Petter and Tyner, 2014; Q: Suardi et al., 2020; R: Vávrová and Knápek, 2012; S: Dieste et al., 2019; T: UNECE, 2020).

	Gasification					
	Switchgrass	**Corn Stover**	**Wheat Straw**	**Miscanthus**	**Pine Bark**	**Spruce Bark**
Price (€/$t_{Biomass}$)	65[G]	83[P]	50[Q]	91[R]	75.41[K,L,S]	20.35[M,N,O,T]
Product cost (€/kg_{MetOH})	0.192	0.216	0.170	0.224	0.169	0.110
Investment (M€)	181.27	175.09	157.67	172.27	144.16	152.79

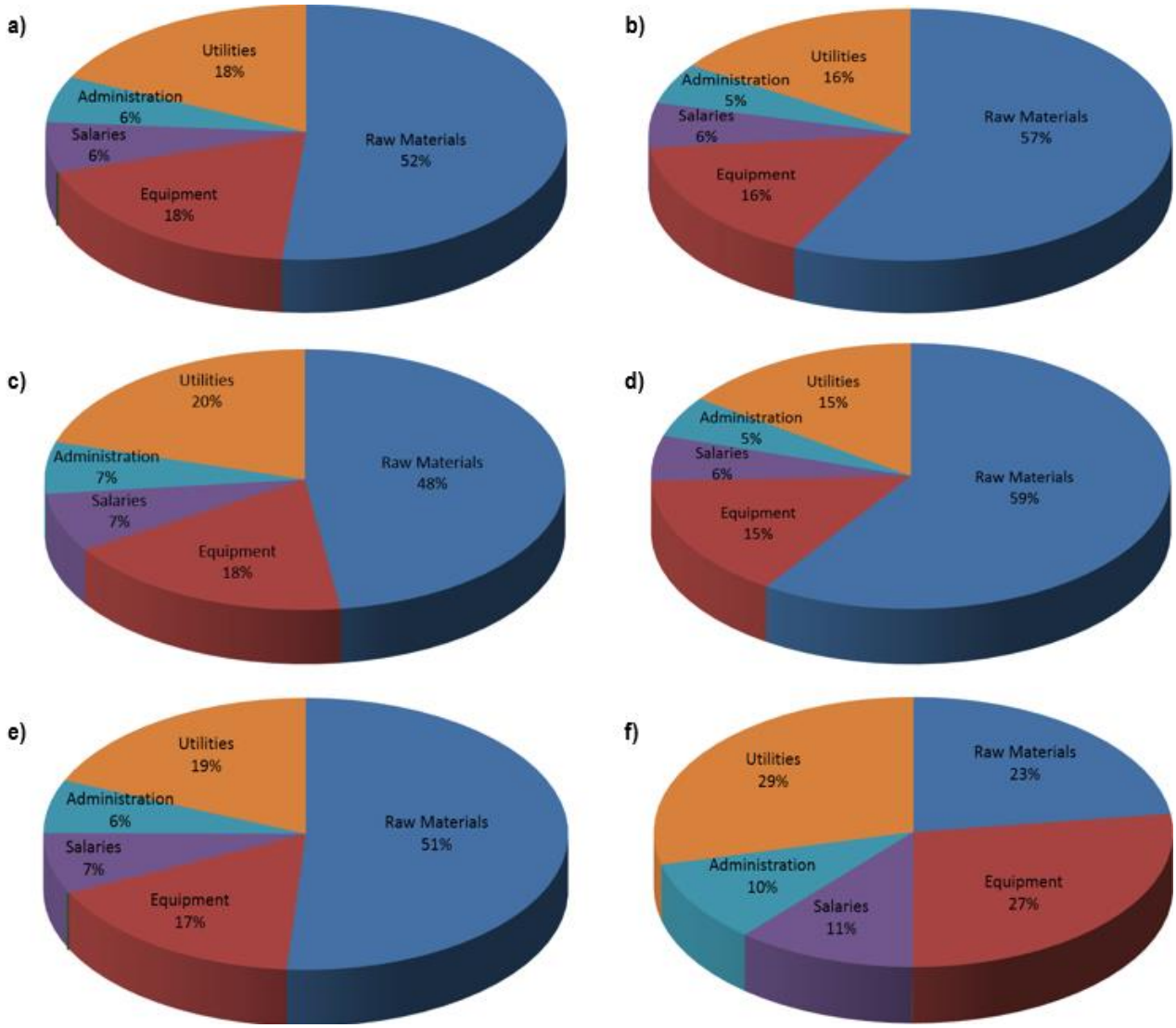

Fig 5. Detailed production costs of the gasification of different biomasses: switchgrass (a), corn stover (b), wheat straw (c), miscanthus (d), pine bark (e), and spruce bark (f).

DAC processes are analyzed as a function of the capture technologies and energy source, either wind or solar. Table 6 summarizes the product and investment cost for conventional processes and BPMED using PV panels and wind turbines. Generally, with the same value of plant investment, the PV panels provide lower costs compared to wind turbines. This can be explained because a part of the cost is associated with the surface that is acquired for the installation of both technologies. The wind turbines need a significant separation between them to avoid interferences, losses of efficiency, and damages to mechanical elements. In addition, the installation and maintenance process is more significant in the case of wind turbines than for PV panels.

However, the decisive factor is the place chosen to situate the installation. Depending on the place, the solar irradiance and the wind speed will vary and consequently the necessary surface of PV panels and the number of wind turbines. From an operational point of view, independently of technology employed to obtain energy, the investment cost of the plant is higher in the BPMED than the conventional process. BPMED employs a considerable amount of electricity in the cells to recover the CO_2 from the solution. This is due to the low ionic concentration of KOH and HCO_3^- and CO_3^{2-}, that energetically reduces the efficiency of the membrane and, with this, the spending of electrical energy. Between these technologies, the lowest production and investment cost corresponds to the conventional process employing PV panels to produce energy, being 0.934 €/ kg_{MetOH} and 1,409.31 M€ (composed by 959.45 M€ of the plant and 449.86 M€ of PV panels). These values represent almost 9 or 10 times larger than the values obtained for the best biomass.

Attending to Figure 6 a and c, and Figure 7 a and c, it can be seen the distribution of production costs, where the equipment represents more than 50%, except for conventional process using PV panels with the lower value, 48%. Figure 6 b and d and Figure 7 b and d show the distribution of investment costs, where the PV panels represent almost 30% while the wind turbines represent values around 40%. Moreover, the conventional process (Figure 4 b and d) presents the lowest percentages concerning fans, 20%, and 17%, respectively. Thus, based on the major yields (Table 4) and the lowest production and investment cost (Table 6), the best process to capture CO_2 from the air is the conventional process using PV panels, for Cádiz. The breakdown of the investment in equipment shows that the items destined to fans, such as PV panels and water electrolysis, represent close to 90% of the total investment cost, leaving as a result only the remaining 11% that can be used for both to the capture of CO_2 and as the synthesis of methanol. The cost of this process would be reduced by improving the efficiency of the photovoltaic panels. As a consequence of this, the number of panels to be used and the total area required would also be reduced.

Table 6.- Production costs and investment for DAC process paths

		DAC			
		Conventional Process PV panels	Conventional Process Wind	BPMED PV panels	BPMED Wind
Product cost (€/kg_{MetOH})		0.934	1.089	1.059	1.233
Investment (M€)	Plant	959.45	959.45	1,218.75	1,218.75
	PV/Wind turbines	449.86	685.50	503.83	767.75

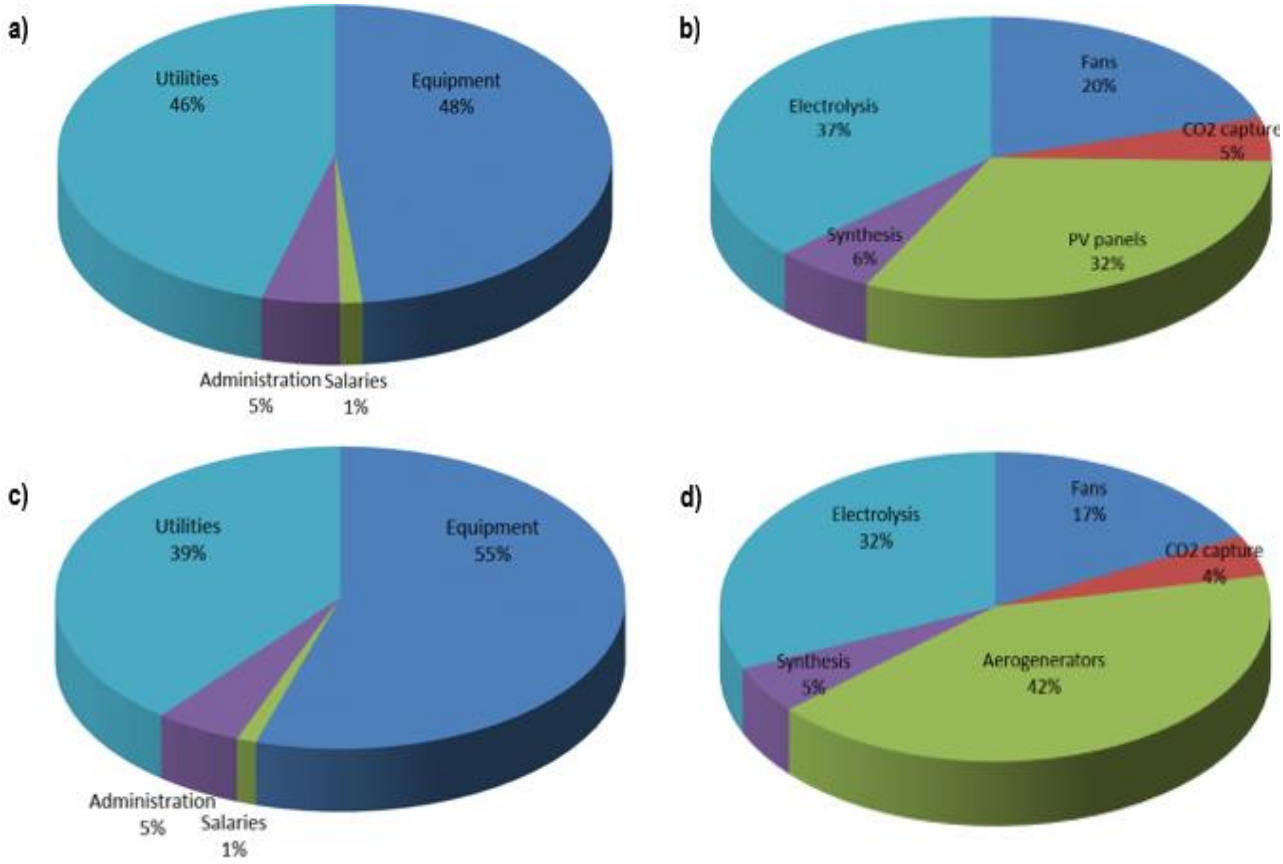

Fig 6. Detailed production and investment costs for conventional DAC PV panels (a production and b investment costs) and DAC wind turbines (c production and d investment costs).

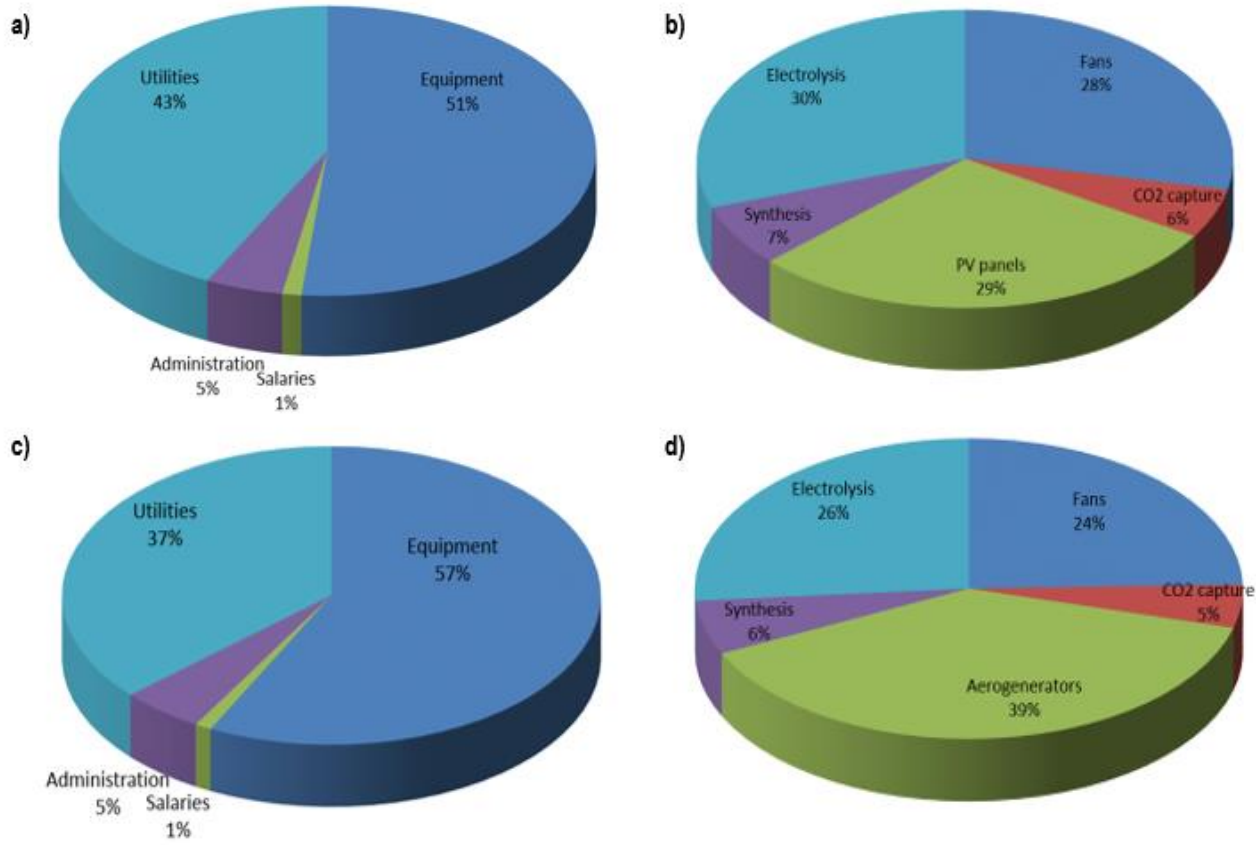

Fig 7. Detailed production costs and investment costs for BPMED process PV panels (a and b).and BPMED process wind turbines (c and d).

5.3.- Sensitivity analysis

This section focuses on the conventional DAC process to evaluate the effect of the variation of the investment cost in PV panels and wind turbines in the final cost of methanol. The base case for PV panels and wind turbines considers 1,050 €/kW and 1,600 €/kW respectively. The base price of methanol is around 0.4-0.7 €/ kg_{MetOH} (Methanol Institute, 2022). Under the current prices for the energy collecting devices (Table 6) the methanol production cost is 2-3 times more expensive. By varying the cost of both energy sources, it is determined that for a price of 100 €/kW the production cost achieved would be 0.670 €/ kg_{MetOH}, being almost within the range of the market price but still far from being competitive.

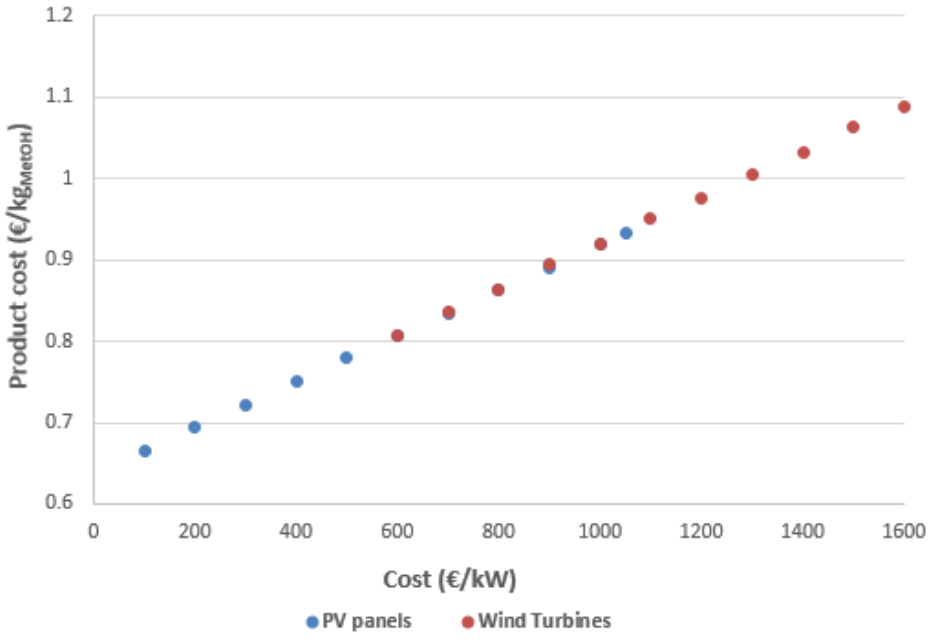

Fig 8. Sensitivity analysis for the methanol production cost with PV panels and wind turbines

6.-Conclusions

This work presents the systematic comparison of CO_2 capture from the atmosphere through the use of natural-type alternatives, biomass growth, and man-made technologies such as direct air capture (DAC), towards the production of a bulk chemical, methanol, in an attempt to achieve a sustainable chemical industry. The optimization of two different DAC configurations is carried out, either by the use of alkaline-type solutions or the use of membranes. These processes make it possible to recover CO_2, which will subsequently be subjected to a hydrogenation stage with hydrogen from water electrolysis. The operation of the installation is based on the use of wind or solar energy, which will be determined by the conditions of the place where the installation is located, in this case, the province of Cádiz (Spain). This CO_2 capture technology is compared to Nature's alternative based on the biomass capture of CO_2. Different biomass species are evaluated, considering switchgrass, corn stover, wheat straw, miscanthus, and forest residues of spruce and pine bark. The biomass that is collected is fed to a process that uses indirect gasification, followed by a steam reforming stage, cleaning the synthesis gas produced and adjusting its composition to carry out the synthesis of methanol.

The most economical alternative to eliminate CO_2 from the atmospheric air consists of the gasification of the biomass of the spruce bark, presenting the lowest production and investment costs, 0.110 €/ kg_{MetOH} and 153 M€ respectively, and one of the highest yields towards methanol, 0.816 $kg_{MetOH}/kg_{biomass}$. Wheat straw could be used as a substitute for spruce bark if not only the price but also the required area is considered as the decisive factor. The technologies based on the DAC process still have production and investment costs around ten times higher than spruce bark gasification. Costs would be greatly reduced with an increase in the performance of PV panels, wind turbines, and improvements in the CO_2 capture system, since if current efficiencies are maintained, it would be necessary to reduce the cost of these technologies almost 90% to obtain a production cost close to 0.670 €/ kg_{MetOH} (Figure 8). This price is still far from competitive.

7.- Nomenclature

A	Parameter 1 of the shape and the conductivity of the bubbles (1.5)
a	Parameter 1 of the wind turbine power equation (8.322 m/s)
B	Parameter 2 of the shape and the conductivity of the bubbles (0.67)
c	Concentration of a chemical in the solution (mol/L)
D	Depth of the packed tower (m)
E	Fitting parameter of Kolhrausch law ($(S \cdot L^{1/2})/(m^2 \cdot mol^{3/2})$)
E_{cell}	Water-splitting potential of the BPM (1.2 V)
E_{BP}	Voltage drop across the BPMED cell (V)
F	Faraday constant (96.500 C/mol)
i	Current density employed in the membrane (A/m^2)
ΔH	Reaction enthalpy (kJ/mol)
J_{CO2}	Molar flow rate of CO_2 through the membrane (mol/s)
$J_{Biomass}$	Set of components for biomass gasification process
$J_{Direct\ air\ capture}$	Set of components for Direct Air Capture process
k^*_{Acid}	Electrical conductivity of the acid solution under CO_2 bubbles effect (S/m)
$k_{solution}$	Electrical conductivity of the acid or basic solution (S/m)
K_1	First equilibrium constant for CO_2 (mol/(L·bar))
K_2	Second equilibrium constant for CO_2 (mol/L)
K_3	Third equilibrium constant for CO_2 (mol/L)
K_H	Henry constant for CO_2 (mol/(L·bar))
K_w	Ion-product constant of liquid water (mol^2/L^2)
N_{cell}	Number of single cells
N_{panel}	Number of PV panels
N_{stackl}	Number of stacks
m	Parameter 2 of the wind turbine power equation (0.806 s/m)
$m_{Cooling\ Needs}$	Mass flow of cooling needs of water (kg/s)

$m_{Evaporated\ Water}$	Mass flow of evaporated water (kg/s)
m_i	Mass flow of component i (kg/s)
$m_{Utilities}$	Mass flow of utilities (kg/s)
P	Power generated by PV solar or wind energy (kW)
ΔP	Pressure drop in the packed tower (Pa)
P_{CO_2}	Partial pressure of CO_2 in the atmospheric air (bar)
P_{Cell}	Power consumption of the single cell (W)
$P_{Electricity}$	Price of the electricity ($1.7 \cdot 10^{-8}$ $/J)
$P_{Nominal}$	Nominal power of a wind turbine (1500 kW)
P_{panel}	Nominal power of a PV panel (8kW)
$P_{Utilities}$	Price of the utilities (19 $/t steam-0.057 $/t cooling water)
P_i	Sale price of component i (€/kg-$/kg)
Q_{air}	Volumetric flow rate of atmospheric air (m^3/s)
R_{Acid}	Electrical resistance of the cell acid compartment (Ω/m^2)
R_{AEM}	Electrical resistance of the AEM membrane ($4.1 \cdot 10^{-4}$ Ω/m^2)
R_{Base}	Electrical resistance of the cell basic compartment (Ω/m^2)
R_{Cell}	Electrical resistance of a unit area of the single cell (Ω/m^2)
$R_{solution}$	Electrical resistance of the acid or basic solution (Ω/m^2)
S	Area of a single membrane (m^2)
SPEND	Specific Energy Demand (kJ/mol_{CO2})
T	Operating temperature (ºC)
ΔT	Variation of temperature between the inlet and outlet cooling water (8ºC)
v	Air velocity (m/s)
$W_{Consumed}$	Electrical power consumed (kW)
W_{fans}	Electrical power involved in fans (MW)
Z	Objective function

Symbols

γ	Parameter for the bubbles effect in the electrical conductivity of the acid compartment
δ	Distance between the BPM and the AEM ($7.62 \cdot 10^{-6}$ m)
ε	Fan electrical efficiency (68.5%)
η	Current efficiency of the membrane (%)
η_{panel}	Efficiency of PV panels (%)
λ_i^o	Molar conductivity of the ion i at infinity dilution($S \cdot m^2 \cdot mol^{-1}$)
Λ_m	Molar conductivity of the solution ($S \cdot m^2 \cdot mol^{-1}$)
Λ_m^o	Molar conductivity of the solution at infinity dilution($S \cdot m^2 \cdot mol^{-1}$)
ν_i	Number of ions i
φ_{co_2}	Volumetric fraction of CO_2 bubbles in the acid solution
φ_m	The maximum value of the volumetric fraction of CO_2 bubbles in the acid solution (0.637)
[]	Concentration (mol/L)

Appendix

Wa: Water
Air: Atmospheric air
Ash: Ash
C: Atomic carbon
H: Atomic hydrogen
N: Atomic nitrogen
O: Atomic oxygen
S: Atomic sulfur
CO_2: Carbon dioxide
CO: Carbon monoxide
H_2CO_3: Carbonic acid
O_2: Oxygen
H_2: Hydrogen
N_2: Nitrogen
CH_4: Methane
C_2H_2: Ethyne
C_2H_4: Ethylene
C_2H_6: Ethane
C_6H_6: Benzene
H_2S: Hydrogen sulfide
MetOH: Methanol
NH_3: Ammonia
CaO: Lime
$Ca(OH)_2$: Calcium hydroxide
$CaCO_3$: Calcium carbonate
KOH: Potassium hydroxide
SO_2: Sulphur dioxide
$(HCO_3)^-$: Bicarbonate ion
$(CO3)^{2-}$: Carbonate ion
OH^-: Hydroxide ion
Tars: Tars
Olivine: Olivine

Indexes

l
f

Supporting Information

Data regarding the development of models, adjustments, and the results of the cost of the different biomasses and direct air capture processes can be found in the supporting information. This material is available free of charge via the Internet at http://pubs.acs.org.

Acknowledgments

The authors thank the PSEM3 GIR group at USAL and the CAPD at CMU. Guillermo Galán appreciates the FPU Ph.D. fellowship from the Spanish Government.

References

[1]. https://www.epa.gov/ghgemissions/overview-greenhouse-gases

[2]. NETL (2014). CO_2 utilization focus area.

[3]. Kondratenko, E.V.; Mul, G., Larrazábal, J.; Baltrusaitis, G.O.; Pérez-Ramírez, J. Status and perspectives of CO_2 conversion into fuels and chemicals by catalytic, photocatalytic, and electrocatalytic processes Energy Environ. Sci. **2013**, 6, 3112 –3135

[4]. Davis, W.; Martín, M. (a). Optimal year-round operation for methane production from CO_2 and Water using wind and/or solar energy. J. Cleaner Prod. **2014**, 80, 252-261.

[5]. Davis, W.; Martín, M. (b). Optimal year-round operation for methane production from CO_2 and Water using wind energy. Energy **2014**, 69, 497–505.

[6]. Martin, M.; Grossmann, I.E. (a) (**2016**). Optimal integration of a self-sustained algae-based facility with solar and/or wind energy Submitted J Clean Prod. 145, 336–47.

[7]. Martín, M. (a). Optimal year-round production of DME from CO_2 and water using renewable energy J. CO_2 Utilization **2016**, 13, 105-113.

[8]. Martín, M.; Grossmann, I.E. On the systematic synthesis of sustainable biorefineries Ind. Eng. Chem. Res. **2013**, 52 (9), 3044-3064.

[9]. Peral, E.; Martín, M. Optimal production of DME from switchgrass-based syngas via direct synthesis. Ind. Eng. Chem. Res. **2015**, 54, 7464-7475.

[10]. Keith, D.W.; Holmes, G.; St. Angelo, D.; Heidel, K. A. Process for capturing CO_2 from the atmosphere. Joule **2015**, 2 (8), 1573-1594.

[11]. Holmes, G.; Keith D.W. An air-liquid contactor for large-scale capture of CO_2 from air. Philosophical Transactions of the Royal Society A: Mathematical, Physical and Engineering Sciences **2012**, 370 (1974), 4380–4403.

[12]. Lackner, K. S.; Ziock, H.; Grimes, P. Carbon Capture from Air, Is It an Option? 24th Annual Technical Conference on Coal Utilization and Fuel Systems **1999**, Clearwater, FL, USA.

[13]. Lackner, K. S. Capture of Carbon Dioxide from Ambient Air. Eur. Phys. J.: Spec. Top. **2009**, 176 (1), 93−106.

[14]. Carey, R; Gomezplata, A.; Sarich, A. An Overview of Submarine CO_2 Scrubber Development. Ocean Eng. **1983**, 10 (4), 227−233.

[15]. Sabatino, F.; Mehta, M.; Grimm, A.; Gazzami, M.; Gallucci, F.; Kramer, G. J.; Van Sint Annaland, M. Evaluation of a Direct Air Capture Process Combining Wet Scrubbing and Bipolar Membrane Electrodialysis. Ind. Eng. Chem. Res. **2020**, 59, 7007−7020.

[16]. Eisaman, M. D.; Alvarado, L.; Larner, D.; Wang, P.; Garg, B.; Littau, K.A. CO_2 separation using bipolar membrane electrodialysis. Energy Environ. Sci. **2010**, 4, 1319–1328.

[17]. Pérez-Uresti S.; Martin M.; Jiménez-Gutiérrez, A. Estimation of renewable-based steam costs. Applied Energy. **2019**, 250, 1120-31.

[18]. Sinnott, R.K. Coulson and Richardson's Chemical Engineering Volume 6, Chemical Engineering Design. Butterworth-Heineman, Oxford **1999**.

[19]. Martín-Hernández, E.; S. Guerras L.; Martín, M. Optimal technology selection for the biogas upgrading to biomethane, Journal of Cleaner Production **2020**, 267, 122032.

[20]. Almena, A.; Martín, M. Techno-economic analysis of the production of epichlorohydrin from glycerol. Ind. Eng. Chem. Res. **2015**, 55 (12), 3226-3238.

[21]. Allen, M.; Dube, O. P.; Solecki, W.; Aragón-Durand, F.; Cramer, W.; Humphreys S.; Kainuma, M.; Kala, J.; Mahowald, N.; Mulugetta, Y. Global Warming of 1.5°C; An IPCC Special Report on the Impacts of Global Warming of 1.5°C above Pre-Industrial Levels and Related Global Greenhouse Gas Emission Pathways, in the Context of Strengthening the Global Response to the Threat of Climate Change, Sustainable Development, And Efforts to Eradicate Poverty; IPPC **2020**.

[22]. Yee, T.F.; Grossmann, I.E.; Kravanja Z.. Simultaneous optimization models for heat integration—I. Area and energy targeting and modeling of multi-stream exchangers. Comp. Chem. Eng. **1990**, 14 (10), 1154-1164.

[23]. Lehninger, A. L.; Nelson, D. L.; Cox, M. M. *Lehninger principles of biochemistry*. New York: Worth Publishers **2000**.

[24]. UN, United Nations Environment Programme 2021. Emissions Report Gap 2021. The Heat is On: A world of climate promises not yet delivered. ISBN: 978-92-807-3890-2. https://www.unep.org/resources/emissions-gap-report-2021

[25]. Seneviratne, S.I.; Nicholls, N.; Easterling, D.; Goodess, C.M.; Kanae, S.; Kossin, J.; Luo, Y.; Marengo, J.; McInnes, K.; Rahimi, M.; Reichstein, M.; Sorteberg, A.; Vera, C.; Zhang X. Changes in climate extremes and their impacts on the natural physical environment. In: Managing the Risks of Extreme Events and Disasters to Advance Climate Change Adaptation [Field, C.B., Barros, V.; Stocker, T.F.; Qin, D.; Dokken D.J.; Ebi, K.L.; Mastrandrea, M.D.; Mach, K.J.; Plattner G.K.; Allen, S.K.; Tignor, M.; Midgley, P.M. (eds.)]. A Special Report of Working Groups I and II of the Intergovernmental Panel on Climate Change (IPCC). Cambridge University Press, Cambridge, UK, and New York, NY, USA, **2012**, 109-230.

[26]. Mbatha, S.; Everson, R.C.; Musyoka, N.M.; Langmi, H.W.; Lanzinid, A.; Brilman, W. Power-to-methanol process: a review of electrolysis, methanol catalysts, kinetics, reactor designs and modelling, process integration, optimisation, and techno-economics. Sustainable Energy Fuels **2021**, 5, 3490-3569.

[27]. Martín, M.; Grossmann, I. E. Optimization simultaneous production of ethanol and i-butene from switchgrass. Biomass Bioenergy **2014**, 61, 93−103.

[28]. Sivasankar, B. Engineering Chemistry. McGraw Hill Education **2008**. ISBN: 0070669325.

[29]. Lide, D.R. CRD Handbook of Chemistry and Physics. CRC Press LLC: Boca Raton **2005**, FL. ISBN: 084930475X.

[30]**.** Seinfeld, J.H.; Pandis, S. N. Atmospheric chemistry and physics: From air pollution to Climate Change. Wiley-Interscience **1997**. ISBN 10: 0471178160.

[31]**.** Sanz-Pérez, M.; Murdock, C.R.; Didas, A.S.; Jones, C.W. Direct capture of CO_2 from ambient air. Chemical Reviews **2016**, 116 (19), 11840-11876.

[32]**.** Pieter Tans, NOAA/ESR **2009**, www.esrl.noaa.gov/gmd/ccgg/trends

[33]. Global CCS Institute. Global status of CCS 2020 report: CCS vital to achieve net-zero.

[34]. Martin, M.; Grossmann, I.E. (b). Towards zero CO_2 emissions in the production of methanol from switchgrass. CO_2 to methanol. Comp. Chem. Eng. **2016**, 105, 308–316.

[35]. Martin M. (b). Methodology for solar and wind-based process design under uncertainty: Methanol production from CO_2 and hydrogen. Comp Chem Eng. **2016**, 92, 43-54

[36]. Eggeman, T. Updated Correlations for GTI Gasifier – WDYLD8. Technical Memorandum for Pam Spath, National Renewable Energy Laboratory **2005**, Golden, Colorado.

[37]. Phillips, S.; Aden, A.; Jechura, J.; Dayton, D.; Eggeman, T. Thermochemical ethanol via indirect gasification and mixed alcohol synthesis of lignocellulosic biomass. Technical Report **2007**, NREL/TP-510–41168

[38]. Martín, M.; Grossmann, I.E. Energy Optimization of Bioethanol Production via Gasification of Switchgrass. AIChE J. **2011**, 57, 12, 3408, 3428.

[39]. Alexopoulou, E.; Zanetti, F.; Papazoglou, E.G.; Iordanoglou, K.; Monti, A. Long-Term Productivity of Thirteen Lowland and Upland Switchgrass Ecotypes in the Mediterranean Region. Agronomy **2020**, 10, 923.

[40]. Khanna, M.; Paulson, N. To Harvest Stover or Not: Is it Worth it? Department of Agricultural and Consumer Economics. Farmdoc Daily **2016**, 6,32.

[41]. Dai, J.; Bean, B.; Brown, B.; Bruening, W.; Edwards, J.; Flowers, M.; Karow, R.; Lee, C.; Morgan, G.; Ottman, M.; Ransom, J.; Wiersma, J. Harvest index and straw yield of five classes of wheat. Biomass and Bioenergy **2016**, 85, 223-227.

[42]. Nolan, A.; McDonnell, K.; Devlin, G.J.; Carroll, J.P.; Finnan, J. Potential availability of non-woody biomass feedstock for pellet production within the Republic of Ireland. Int J Agric & Biol Eng. **2010**, 3(1), 63-73.

[43]. U.S. Department of Agriculture, Forest Service (USDA). Forest Service General Technical Report INT-110. Harvesting and Utilization Opportunities for Forest Residues in the Northern Rocky Mountains **1979**.

[44]. Gryc, V.; Horacek, P.; Šezingerová, J.; Vavrcik, H. Basic density of spruce wood, wood with bark, and bark of branches in locations in the Czech Republic. Wood Research **2011**, 56(1), 23-32.

[45]. Breteau-Amores, S.; Brunette, M.; Davi, H. An Economic Comparison of Adaptation Strategies Towards a Drought-induced Risk of Forest Decline. Ecological Economics **2019**, 164, 106294.

[46]. Liepins, J.; Liepins, K. Evaluation of Bark Volume of Four Tree Species in Latvia. Research for Rural Development **2015**, 2, 22-28.

[47]. Petter, R.; Tyner, W.E. Technoeconomic and Policy Analysis for Corn Stover Biofuels. International Scholarly Research Notices (ISRN) **2014**.

[48]. Suardi, A.; Stefanoni, W.; Bergonzoli, S.; Latterini, F.; Jonsson, N.; Pari, L. Comparison between Two Strategies for the Collection of Wheat Residue after Mechanical Harvesting: Performance and Cost Analysis. Sustainability **2020**, 12(12), 4936.

[49]. Vávrová, K.; Knápek, J. Economic Assessment of Miscanthus Cultivation for Energy Purposes in the Czech Republic. Journal of the Japan Institute of Energy **2012**, 91, 485-494.

[50]. Dieste, A.; Cabrera, M.N.; Clavijo, L.; Cassella, N. Analysis of Wood Products from an Added Value Perspective: The Uruguayan Forestry Case. Maderas. Ciencia y tecnología **2019**, 21(3), 305-316.

[51]. UNECE, United Nations Economic Commission for Europe. Food and Agriculture Organization of the United Nations **2020**. https://unece.org/forests/prices

[52]. SAM **2013** https://sam.nrel.gov/

[53]. Maaßen, M.; Rübsamen, M.; Pérez, A. (**2011**). Photovoltaic Solar Energy in Spain. In: Seminar Papers In International Finance and Economics, Seminar Paper **2011**, 4/2011.

[54]. Goodrich, A.; James, T.; Woodhouse, M. Residential, Commercial, and Utility-Scale Photovoltaic (PV) System Prices in the United States: Current Drivers and Cost-Reduction Opportunities NREL/TP-6A20-53347, February **2012**.http://www.nrel.gov/docs/fy12osti/53347.pdf

[55]. Yimam, Y.T.; Ochsner, T.E.; Kakani, V.G. Evapotranspiration partitioning and water use efficiency of switchgrass and biomass sorghum managed for biofuel. Agricultural Water Management **2015**, 155, 40-47.

[56]. García, J.; Fischer, G.; Riaño, N. Effect of fertilization level on water use and production of corn (*Zea mays* L.) in a cereal producing area in Colombia -a modeling exercise using AquaCrop-FAO. Agronomía Colombiana **2017**, 35(1), 68-74.

[57]. Salim, S. Effect of Water-Retaining Agent (Sky Gel) on Soil Physical Properties, Growth, Yield and Water Use Efficiency of Wheat (Triticum aestivum L.) plant. J.Biol.Chem.Environ.Sci. **2015**, 6(1).

[58]. Dželetović, Z.; Zivanovic, I.; Pivic, R.; Maksimović, J. Water Supply and Biomass Production Miscanthus × giganteus Greef et Deu. Conference: 1st International Congress on Soil Science and XIII National Congress in Soil Science At: Belgrade, Serbia, January **2013**.

[59]. Abad Viñas, R.; Caudullo, G.; Oliveira, S.; De Rigo, D. European Atlas of Forest Tree Species, Pinus pinea in Europe: distribution, habitat, usage, and threats **2016**. ISBN: 9789279367403.

[60]. Bredemeier, M.; Cohen, S.; Godbold, D.L.; Lode, E.; Pichler, V.; Schleppi, P. Forest Management and the Water Cycle: An Ecosystem-Based Approach **2011**. ISBN: 9789048198337.

[61]. León, E.; Martin, M. Optimal production of power in a combined cycle from manure-based biogas. Energy Conversion and Management **2016**, 114, 89–99.

[62]. Perry, R.H.; Green, D.W. Perry's Chemical Engineers' Handbook. New York, McGraw-Hill **1997**. ISBN 10: 0070498415.

[63]. Martín, M.; Martín, M. Cooling limitations in power plants: Optimal multiperiod design of natural draft cooling towers. Energy **2017**, 135, 625-636.

[64]. De la Cruz, V.; Martín, M. Characterization and optimal site matching of wind turbines: Effects on the economics of synthetic methane production. Journal of Cleaner Production **2016**, 133, 1302-1311.

[65]. Agencia Estatal de Meteorología (AEMET) **2020**. http://www.aemet.es/es/portada

[66]. Martín, M. Artifical vs natural reuse of CO_2 for DME production. Are we getting any close? Engineering **2017**, 3(2) 166-170.

[67]. Methanol Institute. Methanol Price and Supply/Demand **2022**. https://www.methanol.org/methanol-price-supply-demand/